Applied Radiation and Isotopes 80 (2013) 49–55

Contents lists available at SciVerse ScienceDirect

Applied Radiation and Isotopes

journal homepage: www.elsevier.com/locate/apradiso

Implementation of gamma-ray spectrometry in two real-time water monitors using NaI(Tl) scintillation detectors

R. Casanovas [a,*], J.J. Morant [b], M. Salvadó [a]

[a] Unitat de Física Mèdica, Facultat de Medicina i Ciències de la Salut, Universitat Rovira i Virgili, ES-43201 Reus (Tarragona), Spain
[b] Servei de Protecció Radiològica, Servei de Recursos Científics i Tècnics, Universitat Rovira i Virgili, ES-43007 Tarragona, Spain

HIGHLIGHTS

- Gamma-ray spectrometry with NaI(Tl) detectors was implemented in two water monitors.
- The monitors were calibrated using experimental data and Monte Carlo simulations.
- The efficiency calculations and MDAC values are given.
- Advantages of using gamma-ray spectrometry are discussed.
- The monitors permit the identification and quantification of isotopes in water.

ARTICLE INFO

Article history:
Received 17 January 2013
Received in revised form
30 May 2013
Accepted 4 June 2013
Available online 13 June 2013

Keywords:
Scintillation gamma-ray spectrometry
NaI(Tl)
Monte Carlo simulation
Efficiency calculation

ABSTRACT

In this study, the implementation of gamma-ray spectrometry in two real-time water monitors using 2 in. × 2 in. NaI(Tl) scintillation detectors is described. These monitors collect the water from the river through a pump and it is analyzed in a vessel, which is shielded with Pb. The full calibration of the monitors was performed experimentally, except for the efficiency curve, which was set using validated Monte Carlo simulations with the EGS5 code system.

After the calibration, the monitors permitted the identification and quantification of the involved isotopes in a possible radioactive increment and made it possible to discard possible leaks in the nuclear plants. As an example, a radiological increment during rain is used to show the advantages of gamma-ray spectrometry. To study the capabilities of the monitor, the minimum detectable activity concentrations for ^{131}I, ^{137}Cs and ^{40}K are presented for different integration times.

1. Introduction

The nuclear power plant in Ascó, Catalonia (ES-E, Spain-East), consists of two pressurized water nuclear reactors cooled with water from the Ebre River. This water is also used for human consumption and crop watering. Thus, to conduct real-time monitoring of the radioactivity levels in water, two monitors have been providing the total gamma activity concentration in water before and after the river passes by both nuclear reactors at Ascó.

However, the obtained radiological values cannot easily be interpreted in terms of the Spanish legislation (Royal Decree 140/2003) (based on the World Health Organization Recommendations (World Health Organization, 2008)) because it fails to consider total gamma activity concentrations. In addition, when some radiological increments occur, it is impossible to distinguish whether they were caused by natural causes (e.g., rain) or artificial emissions (e.g., incidents in nuclear plants). Thus, a previous study identified the implementation of in-situ real-time gamma-ray spectrometry as a possible solution (Casanovas et al., 2011).

The use of gamma-ray spectrometry for real-time water monitoring has become fairly common. Several types of detectors have been used, including NaI(Tl) detectors as the most common example (Bagatelas et al., 2010; Povinec et al., 1996; Tsabaris, 2008; Tsabaris and Ballas, 2005; Tsabaris et al., 2008; Van Put et al., 2004; Vlastou et al., 2006; Vojtyla, 2001; Wedekind et al., 1999), although HPGe (Povinec et al., 1996) and $LaBr_3$(Ce) detectors (Su et al., 2011) have been used as well.

Commonly, real-time water monitoring using gamma-ray spectrometry is conducted by means of direct measurements, i.e. with detectors mounted in floating buoys or with detectors in contact with the sea floor or very close to it (Jones, 2001). When direct measurements are performed, some assumptions concerning the distribution of the source term must be done. Thus, the efficiency

* Corresponding author. Tel.: +34 977759382.
E-mail address: ramon.casanovas@urv.cat (R. Casanovas).

0969-8043/$ - see front matter © 2013 Elsevier Ltd. All rights reserved.
http://dx.doi.org/10.1016/j.apradiso.2013.06.003

calculation is only an approximation that can introduce extra uncertainties in the activity concentrations quantification.

In this paper, the implementation of gamma-ray spectrometry in two river monitors using NaI(Tl) detectors is described. Each of them collect water from the river through a pump and it is analyzed in a vessel. Thus, the counting geometry is always the same and efficiency calibrations can be performed accurately. Besides, the vessel is shielded with Pb, enabling a low background environment that permits better measurement capabilities.

The implementation of gamma-ray spectrometry was conducted through the installation of a parallel spectrometric module in the initial design of the monitor, ensuring its compatibility with other previously installed features. The calibration of the monitor was performed experimentally, except for the efficiency curve, which was set using the Monte Carlo (MC) simulations with the EGS5 code system, which were, in turn, validated with some experimental measurements.

After the presented implementation, the monitor enabled the real-time identification and quantification of radioactive isotope content in the river water. Thus, valuable extra information was obtained at a reasonable cost that guided decisions regarding limits based on current legislation.

2. Materials

2.1. Original system

The original system in both river stations was a Berthold LB/BAI 9110 (Berthold Technologies GmbH & Co. KG, Germany) equipped with a 2 in. × 2 in. NaI(Tl) scintillation detector from ORTEC® (Model 905-3). The system includes a 25 L vessel with a Pb shield (see Fig. 1). A single channel analyzer (SCA) allows one to compute the total concentration of gamma activity (Bq L^{-1}) in water, which is measured real-time and integrated every 10 min.

2.2. New system

To implement gamma-ray spectrometry in the water monitor, a parallel spectrometric module was added to the initial design of the monitor. This module consists of a NaI(Tl) detector and a preamplifier (ORTEC® Model 276) that are connected to an amplifier (ORTEC® Model 575A), which, in turn, is connected to a multichannel pulse-height analyzer (MCA) ORTEC® TRUMP™-PCI-2k.

The spectrometric module was integrated with other previously installed features, resulting in the overall functioning scheme shown in Fig. 2. Thus, the measurement process starts at the vessel (1), where water is collected with a pump from the river. The measurements are conducted with a NaI(Tl) detector (2) connected in parallel to two acquisition cards, an SCA (3) and an MCA (4). The cards are, in turn, connected to their respective associated computers (5) and (6). All data are then transferred to an external server with an SQL database (7) for their storage and processing. An external computer (8) also allows remote interaction with the server or local interaction with the monitor. The system was also improved via the installation of two recipients of 15 L each (9) that can be used to sample water for later analysis in the laboratory. The recipients can be manually or automatically, as well as partially or totally, filled by using several predefined radiological criteria. Finally, the monitor comprises a pneumatic system that allows the insertion and removal of a radioactive test source (10) inside Pb. The source, which can be controlled locally or remotely, can be used to check the spectra stability or energy calibration.

The obtained data are transmitted to the server through an ADSL connection, and the remote control of the system is performed using the TCP/IP protocol. The monitor has different electronic checking sensors that ensure the proper operation of the system. The most relevant are a flow meter (i.e., for the control of the pumped water), a detector temperature probe and an integrated meteorological station (i.e., allowing the measurement of wind speed and direction, as well as air temperature, humidity, barometric pressure, rainfall and solar radiation). From the main

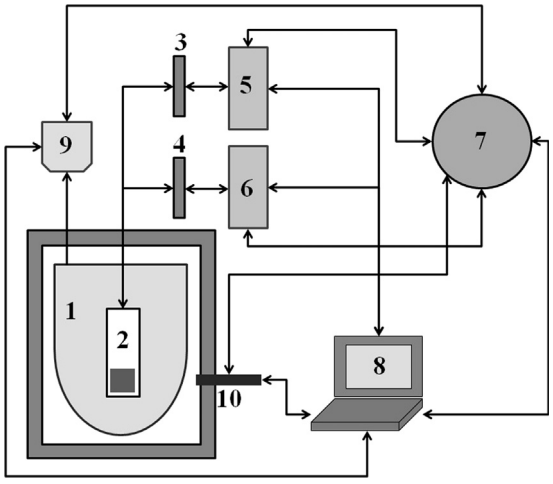

Fig. 2. Schematic showing data acquisition, transfer and processing in the spectrometric water monitoring system. (1) Vessel; (2) NaI(Tl) detector; (3) SCA; (4) MCA; (5) SCA computer; (6) MCA computer; (7) SQL server; (8) external computer; å (9) sampling recipients; and (10) test source.

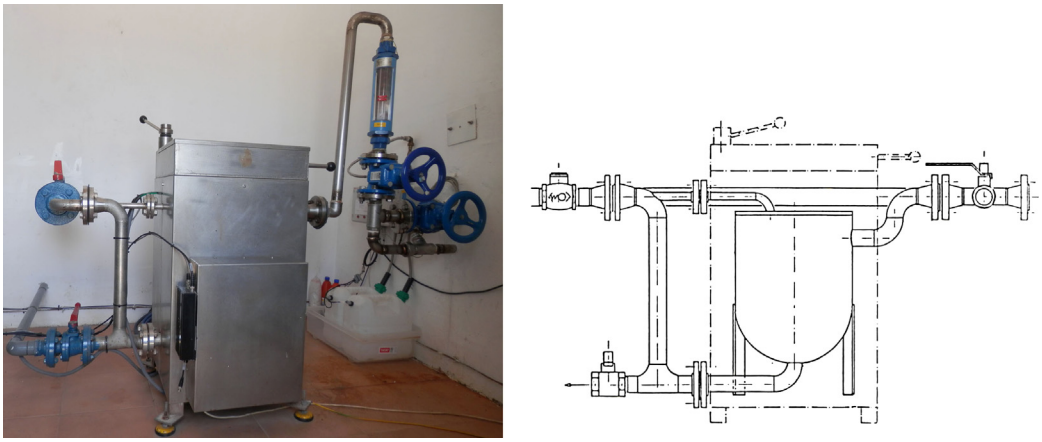

Fig. 1. Image (left) and scheme (right) of the water monitor. The Pb shielding is in the box represented by the dashed lines.

server, it is possible to send automatic messages (SMS or emails) to a predefined contact list, depending on either radiological criteria or different sensor signals.

3. Methods

3.1. Calibration

The calibration methodology for a NaI(Tl) detector has been described in detail in a previous paper (Casanovas et al., 2012a) and adapted specifically for this river monitor. This methodology encompasses energy, resolution and efficiency calibrations.

3.1.1. Energy and resolution calibrations

The energy and resolution calibrations were established using five radioactive point-sources containing ^{241}Am, ^{133}Ba, ^{137}Cs, ^{60}Co and ^{152}Eu. The former was set using the following equation:

$$E = a_0 + a_1 C + a_2 C^2 \quad (1)$$

where C is the channel number, E is the energy and a_k are the fitting coefficients.

The spectra stability is high because the temperature of water varies few along the day. However, to ensure long time measurements, spectra are stabilized. The stabilization is performed fitting a Gaussian curve to the ^{40}K peak at 1460.8 keV to find its position and correcting the entire spectrum using the method described in Casanovas et al. (2012b).

For resolution calibration, the following 2nd-order polynomial was also used to fit the experimental data:

$$FWHM(E) = b_0 + b_1 E + b_2 E^2 \quad (2)$$

where $FWHM(E)$ is the Full Width at Half Maximum, E is the energy and b_k are the fitting coefficients.

3.1.2. Experimental efficiencies

The experimental efficiencies were calculated from the manufacturer's calibration report of the original monitor, which was performed using ^{131}I and ^{137}Cs (364.5 keV and 661.7 keV peaks, respectively). The available data were gross counts in the peak regions instead of net counts under the full-energy peaks. The reported background values were low enough to distinguish any discrepancies between them. However, the discrepancies between net areas and gross areas in normal operation spectra are around 20% as a consequence of the different Compton events that occurred in the crystal. And thus, we assumed an uncertainty level of 20% in the experimental data to account for this deficiency.

To obtain an extra efficiency point at 1460.8 keV, a solution of KCl containing ^{40}K was also prepared. The activity of ^{40}K was estimated from the amount of potassium chloride and its isotopic natural abundance (0.0117%), and the uncertainty was also considered to be 20%.

The experimental efficiencies ε_{exp} were calculated using

$$\varepsilon_{exp} = \frac{N}{A t p_\gamma} \quad (3)$$

where N is the number of the net counts under the full-energy peak, A is the known radionuclide activity, t is the counting time and p_γ is the emission probability of the particular gamma-ray being measured.

3.1.3. Monte Carlo simulated efficiencies

To obtain a complete efficiency curve, efficiency calibration was performed using MC simulations. The MC simulations were performed with a previously validated EGS5 user code (Casanovas et al., 2012a). This user code contains all of the information about the radiation source (diluted in water) and the involved geometry (e.g., vessel, detector, Pb, etc.).

Thus, a model of the monitor was implemented for the MC simulations based on the real dimensions and materials. Fig. 3 shows the implemented geometry model and the materials that were used in each of the regions. The material information (e.g., density and composition) was taken from Berger et al. (2005), and the cut-off energy for the photons and the electrons was set at 10 keV. For the efficiency calculations, each point of the efficiency curve was calculated by considering a monoenergetic source (in the range of 20–2000 keV) that was distributed homogeneously in the water volume. The obtained spectra for the simulated monoenergetic sources were convoluted with the resolution function described by Eq. (2) using the method described in Casanovas et al. (2012a). Then, the broadened spectra were used to calculate the efficiencies using the spectra analysis software ScintiVision™ from ORTEC®.

The efficiency was calculated as

$$\varepsilon_{MC} = \frac{N_{counts}}{N_{hist}} \quad (4)$$

where N_{counts} is the number of net counts under the full-energy peak and N_{hist} is the number of simulated histories (i.e., the

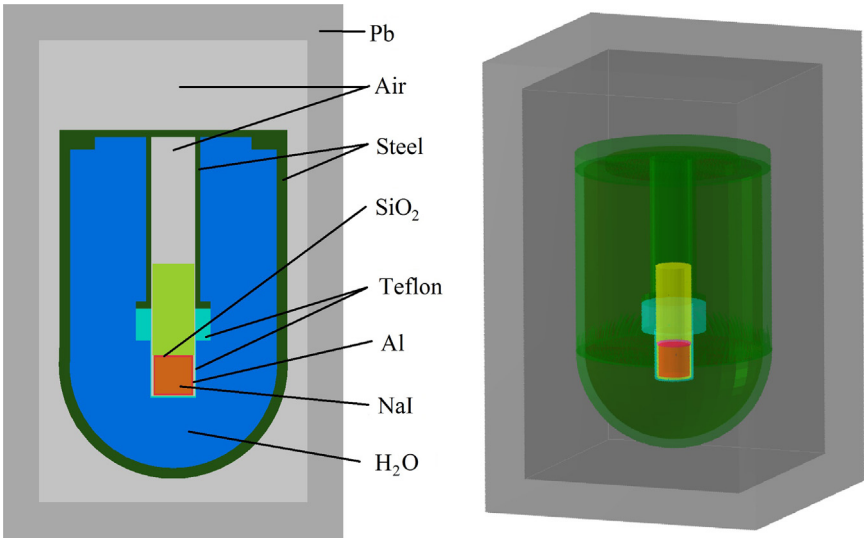

Fig. 3. Geometric model of the monitor (in scale) used in the MC simulations.

number of primary source-particles simulated and all of the secondary particles produced by it), which was set at 10^7.

3.2. Activity calculations

The activity related to each peak was calculated using

$$A = \frac{N}{\varepsilon t p_\gamma} \tag{5}$$

where N is the number of counts under the peak, t is the counting time, p_γ is the emission probability of the gamma-ray and ε is the peak-efficiency.

Using Eq. (5), the activity concentration (e.g., Bq L^{-1}) can be written as

$$a = \frac{N}{\varepsilon_V t p_\gamma} \tag{6}$$

where $\varepsilon_V \equiv \varepsilon V$ is the volumetric efficiency and V is the volume of the vessel, which was 25 L in our case.

3.3. Minimum Detectable Activity Concentration (MDAC)

The detection capabilities of a system are usually evaluated with the detection limit L_D, or the minimum number of counts under a peak that one can be confident of detecting with a certain probability.

Then, the Minimum Detectable Activity Concentration (MDAC) is the activity concentration equivalent to the detection limit L_D. Thus, from Eq. (6) we get

$$MDAC = \frac{L_D}{\varepsilon_V t p_\gamma} \tag{7}$$

If the measured spectrum is assumed to be only background, the detection limit L_D (with a 95% confidence limit) for a certain Region of Interest (ROI) in the spectrum can be calculated using the following single-count Currie expression (Currie, 1968):

$$L_D = 2.71 + 4.65\sqrt{B} \tag{8}$$

where B is the number of counts produced by the background in the considered ROI.

The width of the ROI is determined by the width of the expected peak, which is proportional to the $FWHM(E)$ function

$$n = n(E) = kFWHM(E) \tag{9}$$

where k is the proportionality constant to set the desired peak coverage and $FWHM(E)$ is obtained using Eq. (2). For example, $k = 2.548$ for 99.73% peak area coverage.

4. Results and discussion

4.1. Energy and resolution calibrations

The data used for the energy calibration of the system are shown in Fig. 4. The data were fitted to Eq. (1) and it gave a coefficient of determination of $R^2 = 0.99999$. Similar results were obtained in both monitors, and therefore, only data from one of them are shown.

The maximum relative drift of the ^{40}K peak position is lower than 3% for 1 month period if stabilization methods are not applied. The stabilization method performs well for spectra integrations of 2 h. If shorter integration periods are considered, the location of the ^{40}K peak is not warranted. After the stabilization, the displacement is almost zero and quality of the energy calibration is high.

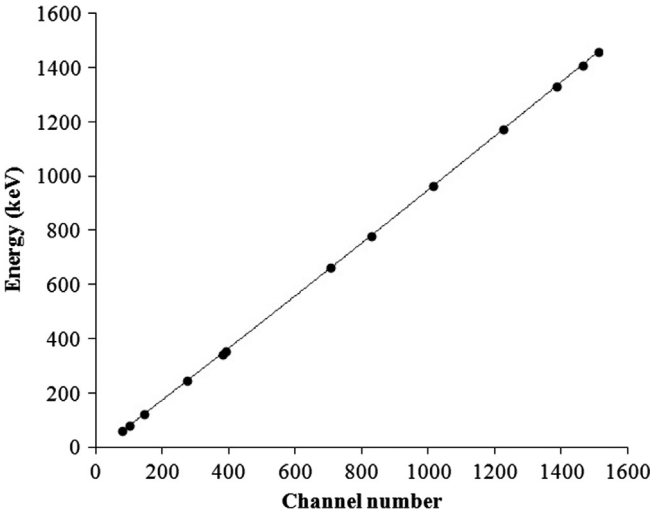

Fig. 4. Energy calibration of the NaI(Tl) detector. The solid line represents the fit of the data to Eq. (1).

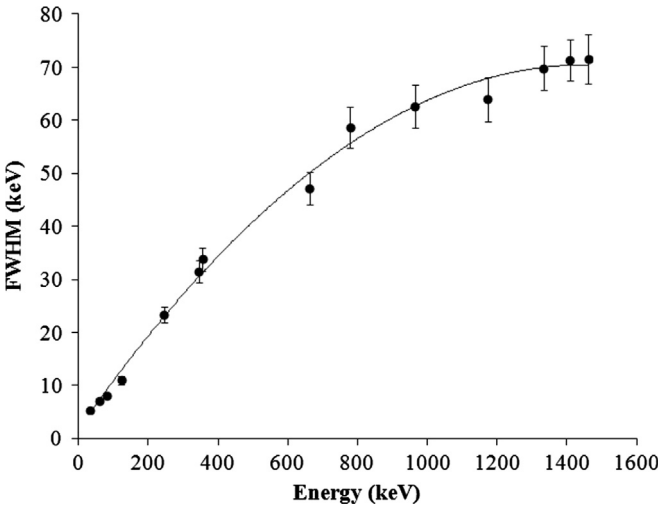

Fig. 5. Resolution calibration of the NaI(Tl) detector. The solid line represents the fit of the data to Eq. (2).

The energy resolution curve was set using Eq. (2) and it gave a coefficient of determination $R^2 = 0.995$. The data used for this calibration together with the statistical uncertainties are drawn in Fig. 5.

4.2. Efficiency calculations

The efficiency curve calculated from the MC simulations and the obtained experimental efficiency values are shown in Fig. 6. The MC simulations provided higher efficiency values than did the experimental measurements. This discrepancy could be attributed to the simplification introduced when modeling the photomultiplier tube, which was assumed to be an aluminum cylinder filled with air. In fact, some tests were performed with different materials inside the photomultiplier that resulted in values closer to the experimental data. In this sense, the geometric model could be improved by studying in detail the structure and materials of the photomultiplier tube. However, as was discussed in Section 3.1.2, the quality of the experimental data was low; thus, before the detector model can be improved, new experimental data must be obtained using certified radioactive solutions.

An uncertainty of approximately 20% in the efficiencies implies an uncertainty of approximately 20% in the activity calculations

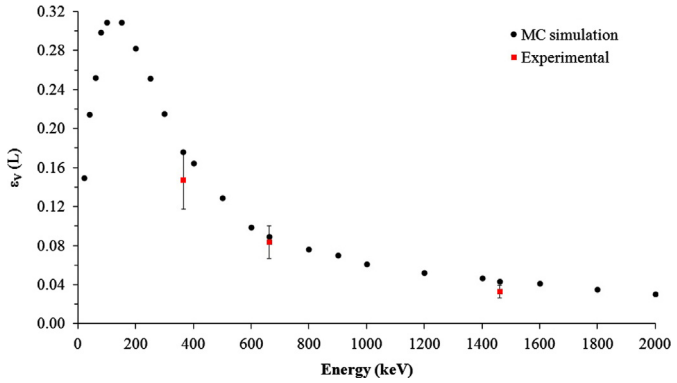

Fig. 6. Efficiency curve calculated using the MC simulations (dots) and experimental efficiencies (squares).

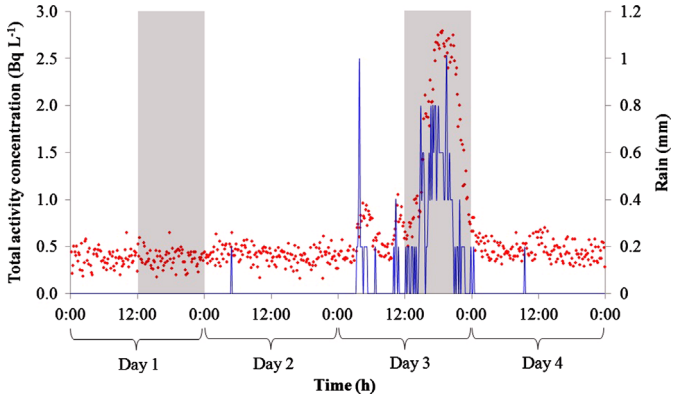

Fig. 7. Radiological increments in the total activity concentration (dots) during Day 3, correlated with rainfall (solid lines). The gray shadows indicate the time intervals considered for the comparison of the 12 h-spectra in Fig. 8.

because the other contributions to the uncertainty are estimated to be lower. Even so, an uncertainty of approximately 20% in real-time spectrometry is assumable because the overall uncertainty can be even higher due to the uncertainty associated with the distribution of the radioactivity in river water, which is assumed to be uniform.

In this sense, the system permits the identification of the isotopes and the estimation of their activity concentration values, which is useful to establish alarm levels. According to this, when significant radiological increments are produced, the monitor has two independent recipients of 15 L each that can sample the water for post-analysis in the laboratory.

4.3. Gamma-ray spectrometry advantages

In this section, an example of the advantages of the implementation of gamma-ray spectrometry is provided. Fig. 7 shows an increment of the total activity concentration in the SCA at Day 3. This radiological increment is clearly time-correlated with a rain episode and was most likely produced by the wash-out of the atmosphere during precipitation. However, it is impossible to know whether it contained an artificial radioactive component.

The data obtained from the spectrometric module provides more radiological information. By way of example, Fig. 8 shows two superposed 12 h-spectra acquired on Day 1 and Day 3, one before the rainfall (Day 1, from 12:00 to 24:00) and the other during it (Day 3, from 12:00 to 24:00). The time intervals of the spectra acquisitions are represented with gray shadows in Fig. 7. The displayed spectra in Fig. 8 are from 2000 channels. The spectra

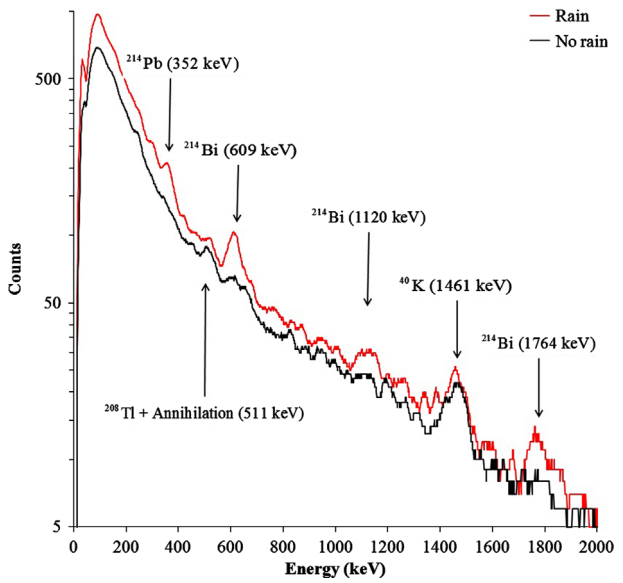

Fig. 8. The 12 h-spectra obtained before the rain episode (Day 1, black lines) and during it (Day 3, red lines). The arrows indicate the isotopes (and their corresponding levels of gamma-ray energy) that produced some of the observed peaks. å(For interpretation of the references to color in this figure legend, the reader is referred to the web version of this article.)

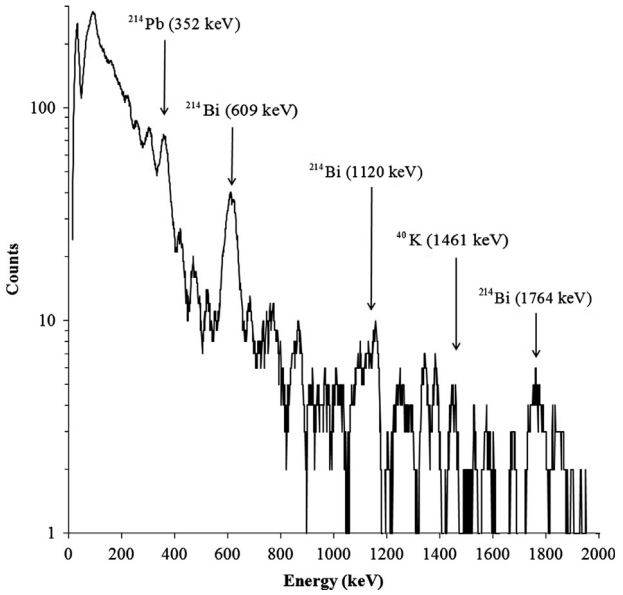

Fig. 9. The subtracted spectrum of Day 3 (rain episode) from the spectrum of Day 1 (normal background). The arrows indicate the isotopes (and their corresponding levels of gamma-ray energy) that produced some of the observed peaks.

were smoothed to depict the peaks clearly. Comparing both spectra, one can clearly see that the radiological increment is basically produced by ^{222}Rn and ^{232}Th daughters (i.e., ^{214}Pb, ^{214}Bi and ^{208}Tl) as a consequence of atmospheric wash-out during the rain. The pure increment produced in this case can be observed after subtracting both spectra (see Fig. 9). The other significant peak that can be observed was produced by the NORM ^{40}K. Hence, because no artificial isotopes were detected, a nuclear plant leak during the rain can be discarded in this case.

4.4. Activity calculations

The activity concentrations of some isotopes are calculated from the 12 h-spectra of Fig. 8. The results of the analysis are

Table 1
Activity concentrations of some isotopes before the rain episode.

Energy (keV)	Isotope	Net area (counts)	Activity concentration (Bq L^{-1})
352	^{214}Pb	480	0.16 ± 0.03
511	^{208}Tl	699	0.6 ± 0.1
609	^{214}Bi	664	0.3 ± 0.1
1120	^{214}Bi	n.a.	n.a.
1461	^{40}K	662	3.3 ± 0.7
1764	^{214}Bi	94	0.4 ± 0.1

Table 2
Activity concentrations of some isotopes during the rain episode.

Energy (keV)	Isotope	Net area (counts)	Activity concentration (Bq L^{-1})
352	^{214}Pb	1403	0.5 ± 0.1
511	^{208}Tl	834	0.7 ± 0.1
609	^{214}Bi	2463	1.3 ± 0.3
1120	^{214}Bi	428	1.2 ± 0.2
1461	^{40}K	742	3.7 ± 0.7
1764	^{214}Bi	279	1.1 ± 0.2

shown in Table 1 (Day 1, before the rain episode) and Table 2 (Day 3, during the rain episode).

In both tables, it can be observed that the ^{214}Pb activity concentration is systematically lower than the ^{214}Bi one, showing a clear disequilibrium between these two ^{222}Rn daughters. The observed increment in the activity concentration of ^{40}K could be attributed to the accumulation of sludge in the vessel, which is frequent during rainfall.

4.5. MDAC

During the day, the variability of the background spectra can be considerable, especially at low integration times. However, regarding the measurement capabilities of the monitor, Table 3 shows the MDAC for the different isotopes and integration times. The spectra are calculated as averages of different spectra (more than 20,000) throughout the day to account for their variability. The MDAC is calculated using Eqs. (7)–(9) (with $k = 2.548$) by assuming that spectra are only background spectra.

The MDAC for ^{40}K was an order of magnitude higher than the MDAC for ^{131}I and ^{137}Cs isotopes because the background spectra have always an important content of ^{40}K. For this reason, the isotopes with energy levels near 1461 keV should be detected using, if possible, other gamma emission lines.

Other MDAC values for 2 in. × 2 in. NaI(Tl) detectors in fresh water were not found in the literature, and thus, direct comparison was not possible. However, the typical MDAC for ^{137}Cs in a 3 in. × 3 in. NaI(Tl) detector measuring directly during 24 h in fresh water is 0.035 Bq L^{-1} (Bagatelas et al., 2010), which is clearly higher than the 0.009 Bq L^{-1} achieved in the 2 in. × 2 in. NaI(Tl) used in the presented monitor. This is an expected result since the Pb shield in the vessel enables lower background measurements in comparison with the other monitor measuring directly in water. Nevertheless, the monitor can only detect those isotopes collected with the pump whereas other monitors measuring directly do not have this restriction.

The monitor capabilities may be improved by using longer and larger NaI(Tl) detectors, which would enable a more efficient system, thus lowering MDACs. Another important improvement to the monitor would be the use of $LaBr_3$(Ce) detectors. These detectors have, in general, worse MDACs compared with NaI(Tl) ones because of their intrinsic self-activity (Su et al., 2011). However, they present good energy resolution that can be an important factor when several isotopes are detected.

Table 3
MDAC for the different isotopes and integration times.

Isotope	Energy (keV)	MDAC (Bq L^{-1})				
		10 min	1 h	4 h	12 h	24 h
^{131}I	364.5	0.9	0.2	0.04	0.01	0.007
^{137}Cs	661.7	1.2	0.2	0.05	0.02	0.009
^{40}K	1460.8	13.2	2.2	0.55	0.18	0.092

5. Conclusions

Two real-time water monitors using 2 in. × 2 in. NaI(Tl) scintillation detectors were improved by installing a gamma-ray spectrometric module, which was implemented to ensure its compatibility with other previously installed features. The new feature provided valuable extra information at a reasonable cost, which enables the establishment of decision limits based on current legislation. The monitors were calibrated using experimental data, except for the efficiency curve, which was set using the Monte Carlo simulations with the EGS5 code system.

The spectrometric module presented clear advantages in comparison with the old system. For example, it enabled the identification of the involved isotopes in radiological increments and made it possible to discard a possible artificial cause. The capabilities of the new monitor were evaluated with some MDAC calculations over average spectra, which showed a good performance, especially for ^{131}I and ^{137}Cs isotopes. In comparison to other monitors that measure directly in water, the obtained MDAC values were lower, and thus, a faster identification can be performed. In addition, the quantification of the activity can be more precise because the counting geometry is always the same and no assumptions about the source term geometry must be done. However, the system can only detect those isotopes collected with the pump and alternative systems measuring directly in the river could be also useful.

As shown via its implementation and calibration, the monitor enables the real-time identification and quantification of radioactive isotope content in river water. This functionality enables a comparison of the obtained data with the legal limits established for the activity concentrations in water, thereby allowing one to establish alarm levels for early warning. As such, valuable extra information could be obtained by comparing both monitors, which are before and after the nuclear plant.

Acknowledgments

Part of this research was performed using the resources of CESCA (Centre de Supercomputació de Catalunya).

References

Bagatelas, C., Tsabaris, C., Kokkoris, M., Papadopoulos, C.T., Vlastou, R., 2010. Determination of marine gamma activity and study of the minimum detectable activity (MDA) in 4pi geometry based on Monte Carlo simulation. Environ. Monit. Assess. 165, 159–168.

Berger, M.J., Coursey, J.S., Zucker, M.A., Chang, J., 2005. ESTAR, PSTAR, and ASTAR: Computer Programs for Calculating Stopping-Power and Range Tables for Electrons, Protons, and Helium Ions (version 1.2.3). National Institute of Standards and Technology, Gaithersburg. Available from: ⟨http://physics.nist.gov/Star⟩.

Casanovas, R., Morant, J.J., Lopez, M., Hernandez-Giron, I., Batalla, E., Salvado, M., 2011. Performance of data acceptance criteria over 50 months from an automatic real-time environmental radiation surveillance network. J. Environ. Radioact. 102, 742–748.

Casanovas, R., Morant, J.J., Salvadó, M., 2012a. Energy and resolution calibration of NaI(Tl) and $LaBr_3$(Ce) scintillators and validation of an EGS5 Monte Carlo user

code for efficiency calculations. Nucl. Instrum. Methods Phys. Res. Sect. A 675, 78–83.
Casanovas, R., Morant, J.J., Salvadó, M., 2012b. Temperature peak-shift correction methods for NaI(Tl) and $LaBr_3$(Ce) gamma-ray spectrum stabilisation. Radiat. Meas. 47, 588–595.
Currie, L.A., 1968. Limits for qualitative detection and quantitative determination. Anal. Chem. 40, 586–593.
Jones, D.G., 2001. Development and application of marine gamma-ray measurements: a review. J. Environ. Radioact. 53, 313–333.
Povinec, P.P., Osvath, I., Baxter, M.S., 1996. Underwater gamma-spectrometry with HPGe and NaI(Tl) detectors. Appl. Radiat. Isot. 47, 1127–1133.
Royal Decree 140/2003 of 7 February by Which Health Criteria for the Quality of Water Intended for Human Consumption are Established. Available from: ⟨http://www.msc.es/profesionales/saludPublica/docs/royal_decree_140_2003.pdf⟩.
Su, G., Zeng, Z., Cheng, J., 2011. Monte Carlo simulation of in situ LaBr gamma-ray spectrometer for marine environmental monitoring. Radiat. Prot. Dosim. 146, 103–106.
Tsabaris, C., 2008. Monitoring natural and artificial radioactivity enhancement in the Aegean Sea using floating measuring systems. Appl. Radiat. Isot. 66, 1599–1603.
Tsabaris, C., Ballas, D., 2005. On line gamma-ray spectrometry at open sea. Appl. Radiat. Isot. 62, 83–89.
Tsabaris, C., Bagatelas, C., Dakladas, Th., Papadopoulos, C.T., Vlastou, R., Chronis, G.T., 2008. An autonomous in situ detection system for radioactivity measurements in the marine environment. Appl. Radiat. Isot. 66, 1419–1426.
Van Put, P., Debauche, C., De Llelis, C., Adam, V., 2004. Performance level of an autonomous system of continuous monitoring of radioactivity in seawater. J. Environ. Radioact. 72, 177–186.
Vlastou, R., Ntziou, I.Th., Kokkoris, M., Papadopoulos, C.T., Tsabaris, C., 2006. Monte Carlo simulation of gamma-ray spectra from natural radionuclides recorded by a NaI detector in the marine environment. Appl. Radiat. Isot. 64, 116–123.
Vojtyla, P., 2001. Calibration of monitors used for surveillance of radioactivity in effluent water from CERN's accelerator installations. Appl. Radiat. Isot. 55, 81–88.
Wedekind, Ch., Schilling, G., Grüttmüller, K., Becker, K., 1999. Gamma-radiation monitoring network at sea. Appl. Radiat. Isot. 50, 73–741.
World Health Organization, 2008. Guidelines for Drinking-Water Quality [Electronic Resource]: Incorporating 1st and 2nd Addenda, Vol. 1. 3rd ed. Recommendations. isbn:9789241547611. Available from: ⟨http://www.who.int/water_sanitation_health/dwq/fulltext.pdf⟩.